applied sciences

MDPI

Article

Investigations on an Ancient Mortar from Ulpia Traiana Sarmizegetusa Archaeological Site, Romania

Zeno Dorian Ghizdavet [1], Corina Anca Simion [2,*], Anton Ficai [1,3], Ovidiu-Cristian Oprea [1,3,4], Radu Claudiu Fierascu [5], Maria Loredana Marin [2], Doina-Roxana Trușcă [4], Vasile-Adrian Surdu [6], Ludmila Motelica [3,4,7], Iuliana Madalina Stanciu [2], Alexandru Razvan Petre [2] and Ileana Radulescu [2]

1 Faculty of Chemical Engineering and Biotechnologies, National University of Science and Technology POLITEHNICA Bucharest, 060042 Bucharest, Romania; zeno.ghizdavet@upb.ro (Z.D.G.); anton.ficai@upb.ro (A.F.); ovidiu.oprea@upb.ro (O.-C.O.)
2 Horia Hulubei National Institute for R&D in Physics and Nuclear Engineering (IFIN-HH), 30 Reactorului St., P.O. Box-MG-06, 077125 Magurele, Ilfov County, Romania; marinmarialoredana@yahoo.com (M.L.M.); iuliana.stanciu@nipne.ro (I.M.S.); alexpetre@nipne.ro (A.R.P.); rileana@nipne.ro (I.R.)
3 Academy of Romanian Scientists, 050044 Bucharest, Romania; ludmila.motelica@upb.ro
4 National Centre for Micro and Nanomaterials and National Centre for Food Safety, National University of Science and Technology POLITEHNICA Bucharest, 060042 Bucharest, Romania; truscaroxana@yahoo.com
5 National Institute for Research and Development in Chemistry and Petrochemistry, 202 Spl. Independentei, 060021 Bucharest, Romania; fierascu.radu@icechim.ro
6 Department of Materials Science, Faculty of Materials Science and Engineering, Transilvania University of Brasov, 29 Eroilor Blvd., 500036 Brasov, Romania; vasile.surdu@unitbv.ro
7 Research Center for Advanced Materials, Products and Processes, National University of Science and Technology POLITEHNICA Bucharest, 313 Splaiul Independentei, 060042 Bucharest, Romania
* Correspondence: anke@nipne.ro

Abstract: A fragment of mortar from the pedestal ruin belonging to the central statue in Forum Vetus, Ulpia Traiana archaeological site, Romania, was investigated. The ruin is well-documented and unrestored, and radiocarbon dating was deemed suitable to determine its moment of construction. Preliminary analyses were used to establish the composition of the material and the sources of carbon-14, selecting the most reliable fraction for radiocarbon dating by the AMS method. Although sampling was carried out according to the recommendations, a younger apparent age was obtained than that expected. This is in fact a concrete-like mortar according to the analyses, and the phenomenon of delayed hardening of mortar in masonry was detected. The difference between the real and apparent ages quantifies this phenomenon. X-ray diffraction, scanning electron microscopy with energy-dispersive X-ray spectroscopy, Fourier-transform infrared spectroscopy, differential scanning calorimetry with thermogravimetric analysis, and gamma spectrometry were used. Pyrogenic calcium carbonate and carbonates from calcium silicate/calcium aluminate hydrates were the only forms present in mini-nodules/lumps. The reactivation of binder calcite or geogenic calcite, the other problems encountered when dating mortars, were not spotted. This case study highlights the limitations of the radiocarbon dating method, and we introduce gamma spectrometry as a technique for additional investigations into direct exposure to the environment or the origins of raw materials.

Keywords: mortar characterization; multi-analytical techniques; carbon-14 dating strategy; apparent radiocarbon age; delayed mortar hardening

Academic Editor: Markssuel Teixeira Marvila

Received: 23 April 2025
Revised: 18 May 2025
Accepted: 20 May 2025
Published: 21 May 2025

Citation: Ghizdavet, Z.D.; Simion, C.A.; Ficai, A.; Oprea, O.-C.; Fierascu, R.C.; Marin, M.L.; Trușcă, D.-R.; Surdu, V.-A.; Motelica, L.; Stanciu, I.M.; et al. Investigations on an Ancient Mortar from Ulpia Traiana Sarmizegetusa Archaeological Site, Romania. *Appl. Sci.* **2025**, *15*, 5780. https://doi.org/10.3390/app15105780

1. Introduction

As of 2024, the ancient civil settlement of Ulpia Traiana Sarmizegetusa was on the list of UNESCO World Cultural Heritage monuments, which includes the Roman settlements on the borders (*Limes*) of the Dacia province.

In this context, the remaining plinth of the central statue in Forum Vetus deserves reconsideration from an archaeological point of view.

From the archaeometrical perspective, there is an opportunity to improve the knowledge on construction materials using modern analytical methods and to assess the reliability and challenges of radiocarbon dating applied to ancient mortars.

Mortars are a wide class of building materials used for more than 8500 years [1,2]. Regardless of their formulation, all mortars are made of binder and aggregates. Materials close to our current understanding of mortars are the pozzolanic mortars that originated in Greece around 500 BC [3]. Romans later improved their use and methods of preparation [4].

Pozzolanic mortars are made of a pozzolanic material (for example, volcanic ash), slaked lime, water, and aggregates. Pozzolanic reaction takes place between a siliceous or siliceous–aluminous pozzolanic material and slaked lime/calcium hydroxide $Ca(OH)_2$ in the presence of water, at ambient temperature, leading to the formation of calcium silicate (C-S-H) and calcium aluminate (C-S-A-H) hydrates, which harden over time [5].

Along with the binder matrix made of hydrated compounds, calcium carbonate $CaCO_3$ can also be found in mortars [6]. $CaCO_3$ in a mortar's binder phase can originate, in significant amounts, from five sources:

(S1) Non-decomposed $CaCO_3$ from the original limestone (geogenic calcite) [7]. This carbonate depends on the processing conditions for obtaining slaked lime and should be minimized, although, in some recipes, it is added intentionally to provide a secondary source of calcite/calcium carbonate, with the idea of regenerating genuine source of carbonates formed by hardening [4].

(S2) $CaCO_3$ from carbonation over time of $Ca(OH)_2$ in excess (pyrogenic calcite); this process may need, for aerial mortars, a carbonation rate of 80–92% after 100 years [8]. It can occur under ambient carbon dioxide concentrations (with different carbon-14/C-14 contents, depending on the historical period), being thermodynamically favored (exothermal reaction). It is optimal for dating construction segments because it reflects the $^{14}CO_2$ level for the construction or restoration time [9].

(S3) $CaCO_3$ from carbonation of C-S-H hydrates areas of formation (C-S-H carbonation) [10]; this specific carbonation can take a variable number of years, depending on microstructural features, weather conditions, microstructure evolution due to micro-cracking, and weathering [11,12]. The degree of carbonation of the cementitious materials is, usually, estimated by the measurement of carbonation depth [12]. Various polymorphs of calcium carbonate, along with S-H/S-A-H and water, are the products of this carbonation process.

(S4) $CaCO_3$ can be also obtained via recarbonation of $Ca(OH)_2$ ($Ca(OH)_2$ recarbonation); over time, a fraction of S1–S3 calcite may eliminate carbon dioxide by dissolution, leading to calcium hydroxide. $CaCO_3$ regeneration will take place by precipitation using a proximal CO_2 source with a different C-14 signature (older or younger than genuine calcium carbonate formed by hardening) [13,14].

Calcium carbonate/calcite, obtained from the S1–S4 sources, will have different levels of carbon-14. Due to its origin and mechanisms of formation, it presents distinct physical and chemical properties and can be separated under certain conditions as fractions. Differentiation between fractions can be achieved using Accelerator Mass Spectrometry, highlighting the formation pathways [13]. From the geomorphological point of view, calcium carbonate is distributed in nature in three mineral forms: calcite, aragonite, vaterite. Although vaterite can also form in anthropogenic materials such as mortar, it is unsta-

ble. Aragonite, on the other hand, can be identified [15]. However, if it is highlighted by methods of analysis prior to radiocarbon dating, it can be removed [16].

Mortar maturation means that all these processes have been completed, and an equilibrium reached, long before analyses. The analyses can establish the occurrence of ripening, and also the presence or absence of recarbonation phenomena [13].

Aggregates constitute a major part of mortars/concretes; ancient pozzolanic mortars were made with natural aggregates, such as sand, limestone, and mussel shells [17], or artificial aggregates, such as crushed ceramics, which contain aluminosilicates as a pozzolanic material [18,19]. When using quarry sand/beach sand or even that from riverbeds, a fifth category of carbonates may appear, which can seriously affect the radiocarbon data these are carbonate deposits/calcareous concretions (S5) (calcareous concretions) [20].

During formation, porosity plays an important role in carbonation. Pores have a wide range of sizes and shapes in mortars/concretes. Coarse pores greater than 100 μm in diameter are usually formed by the following [17]: (i) *entrapped air*, formed by entrapment of air during mixing. They present both irregular shapes and distributions (and can serve as the primary source of carbon dioxide, at a C-14 level very close to the time of manufacture); (ii) *entrained air pores* are round voids formed by organic materials, some of them containing proteins, presenting bubble-like shapes (carbon dioxide will result from the decomposition of organic matter usually close in time to the manufacturing moment). Coarse pores contribute negatively to the strength of the mortar, along with cracks that can occur due to weathering, mechanical actions, and/or chemical reactions, which lead to the formation of higher-molar-volume compounds (developing internal stress that can lead to cracking). By these means, carbon dioxide of a much younger age than the building can appear in a proportion determined by the depth profile toward the building surface.

Interconnected capillary pores contribute to water and air/CO_2 transfer, with their specific formation making a positive contribution to the strengthening of the mortar over time and to its self-regeneration [4]. In lime-based mortars, pores smaller than 0.1 μm are present in limited amounts and can be identified in hydrated phases. Intermediate-sized pores, of around 50 μm, can be formed between the binder and the aggregate, though decreasing mortar strength. The carbonation reaction of $Ca(OH)_2$ in mortars is possible if a free pathway exists for water and CO_2 to coexist at the carbonation site. The consequence for ancient lime mortars is that the radiocarbon dating result may be highly dependent on the carbonation depth, the weather conditions, and the air/water/CO_2 mass transfer within a given mortar's system of pores. The age of carbonation can vary with depth and position (due to the porosity features of a given volume). Also, low amounts of contaminating carbon-bearing compounds (older/younger ^{14}C in organic or inorganic compounds with different radiocarbon ages) can be attributed to complex interactions over time: chemical and biochemical degradation, meteoric waters, human impact, etc. [21,22].

With increasing age, the microstructure become denser due to calcium carbonate particles increasing in number and size, thus occupying some of the pores [23].

The aim of the present article is to reveal all these interactions and C-14-bearing sources by investigating a mortar collected from the archaeological site Ulpia Traiana, Romania. This was achieved by testing the limitations of analytical methods used in the material characterization of whole mineral fractions and of lump fractions of well-documented archaeological remains.

Through a set of instrumental analyses, the degree of maturation, the presence/absence of S1–S5 calcite sources described above, and occurrence of calcium hydroxide were investigated in relation to the radiocarbon results.

Last but not least, this article shows to what extent, even if sampling is carried out according to the requirements, in the case of concrete-like mortars, a situation arises of

radiocarbon ages that differ from the estimates. This is the phenomenon of 'delayed-hardening mortar', where the material hardens very slowly, providing much younger radiocarbon ages.

2. Materials and Methods

2.1. Materials

The material to be investigated (Figure 1) came from Ulpia Traiana, an important archaeological complex situated in southwestern modern-day Romania, extracted from the remaining plinth of the central statue in Forum Vetus (Figure 2). Although the size of the aggregates qualifies the material as being a 'concrete' rather than a 'mortar', the term 'mortar' will be used in this paper to refer to an ancient, lime-based construction material.

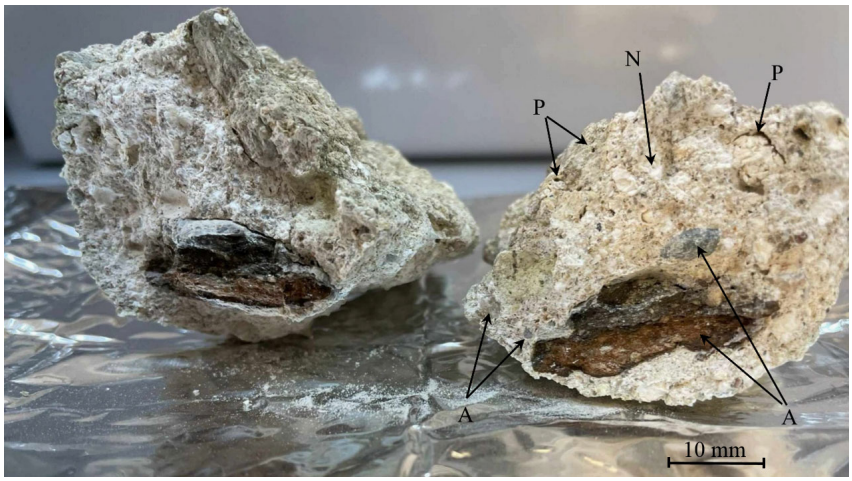

Figure 1. Mortar specimens containing $CaCO_3$ nodules (N), aggregates (A), and pores (P); extracted from below the exposed surface.

Figure 2. Forum Vetus, Colonia Ulpia Traiana Augusta Dacica Sarmizegetusa; the remains of the statue's plinth.

A visual inspection identified 2–3 cm aged gneiss aggregates along with a wide range of other aggregates (up to 10 mm in size but most of them under 1 mm) well connected to the matrix, embedded in a mortar containing a large number of millimeter-sized, relatively uniformly dispersed, $CaCO_3$-rich white areas, giving a first confirmation of the age of the material. Cracks and mostly rounded, closed macroscopic pores were also visible.

To obtain fresh surfaces in order to eliminate, as much as possible, the influence of weathering, the samples were sliced with an angle grinder. Microscopic images show an almost unaffected surface (only a few small aggregates were extracted, while the larger ones were sliced through), suggesting that a strong bond between aggregates and the binder matrix still exists, even after the mechanical action; also, large carbonation areas can be easily identified (Figure 3). Beyond the surface exposure, the material has a well-connected structure in which there are large areas of carbonation products that have occupied the available pores over time. This shows that the material can provide a datable carbon source through these carbonation products, and that in those areas, this process ended a long time ago.

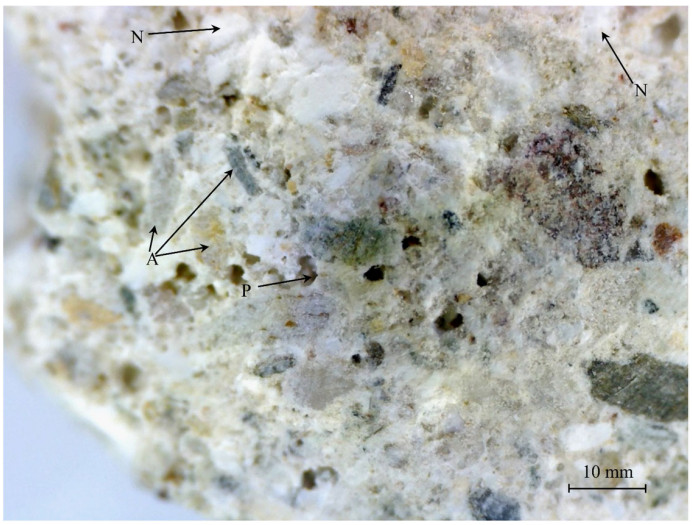

Figure 3. Various natures and sizes of aggregates, pores, and carbonates (dusty white) in sliced, freshly made surface (N—nodules; A—aggregates; P—pores).

No carbonate concretions that could come from aggregates were identified in the analyzed sample, so the S5 calcareous concretion mechanism was discarded.

2.2. Methods

The material was initially characterized by microscopy; X-ray diffraction (XRD); scanning electron microscopy with energy-dispersive X-ray spectroscopy (SEM-EDAX); Fourier-transform infrared spectroscopy (FTIR); differential scanning calorimetry with thermogravimetric analysis (DSC-TGA); and gamma-ray spectrometry. Technical information about the equipment used is provided in Appendix A.

For gamma spectrometry analyses, detector calibration for the energy scale and efficiency was accomplished using traceable volume standard sources [24]. Spectral data were collected over a long live time of 356,000 s, in order to achieve a low detection limit.

According to the recommendations in the literature, and the conclusions drawn from the previous analyses of the material, the selection of samples to be dated using the radiocarbon method was oriented towards the identification and extraction of mini-nodules, 2–3 mm in size, defined as 'lumps and bumps' [7,25]. The chemical release of CO_2 from $CaCO_3$ was achieved primarily through chemical digestion with ortho-phosphoric acid, in the Carbon Handling System (CHS) installation, followed by the separation/purification of the gas and its reduction to carbon in the AGE 3 graphitization unit [26] (Ionplus, Dietikon, Switzerland). C-14 level determination in the carbon, intimately deposited on the iron catalyst, was carried out using the AMS method in the 1MV HVEE particle accelerator [27] (High Voltage Engineering Europa B.V., Amersfoort, The Netherlands). The transformation

of raw data to the Conventional Radiocarbon Age (CRA), in years BP, was performed using an adapted version of the BATS Program version 4.06 (04.06.2015) written by L. Wacker [28], and finally the calendaristic years calAD were obtained using OxCal curves, version 4.4.4 [29]. To verify the calibrated age, a second target (carbon deposited on iron) was obtained from the remaining extracted portion of mini-nodules (lumps and bumps), but this time using thermal CO_2 generation, in an Elemental Analyzer (EA, VarioMicroCube, Elementar, Hanau, Germany) [30]. The other stages proceeded similarly to the first dating attempt.

The literature suggests a separate collection of CO_2 fractions from carbonates of different ages (coming from S1–S5 sources), and their individual dating if they come from lime binder [31]. This is not possible using the CHS, and the radiocarbon data from samples that undergo combustion in the EA must also be viewed with circumspection. For lime lumps, only one fraction is generally dated (if no secondary calcite is present and if they are not underburned). That is why the series of methods described above for characterizing the initial sample was used not only for material characterization but also for the radiodating strategy. Thus, there is a chance to choose the best sub-samples and also to correctly interpret the obtained radiocarbon data. If the contamination sources S1 geogenic calcite, S4 $Ca(OH)_2$ recarbonation, and S5 calcareous concretions are not highlighted, then the possible age difference between the calcite formed by S2 pyrogenic calcite and/or S3 C-S-H carbonation matters less. Given the interval in which the statue could have been built (in less than a 150-year interval), as in the case of some Roman mortars, the second fraction may be more reliable [6]. Thus, the whole fraction when using the CHS can provide a result that can be interpreted.

A schematic workflow is given in Appendix B.

3. Results

3.1. XRD Analysis

The XRD analysis results in Figure 4 show that the mortar is rich in the feldspar mineral albite ($NaAlSi_3O_8$—ICDD PDF4+#00-009-0466), indicating an igneous origin (granite, locally available) of the siliceous component in the original mortar mixture. Quartz (SiO_2—ICDD PDF4+#01-070-3755) and calcite ($CaCO_3$—ICDD PDF4+#04-023-8700) follow albite in similar percentages, while a small amount of kaolinite ($Al_2O_3 \cdot 2SiO_2 \cdot 2H_2O$_ICDD PDF4+#00-058-2028) was found. Kaolinite may be used as an ingredient deliberately or accidentally released in the original mortar admixture and/or may be a contaminant accumulated over time.

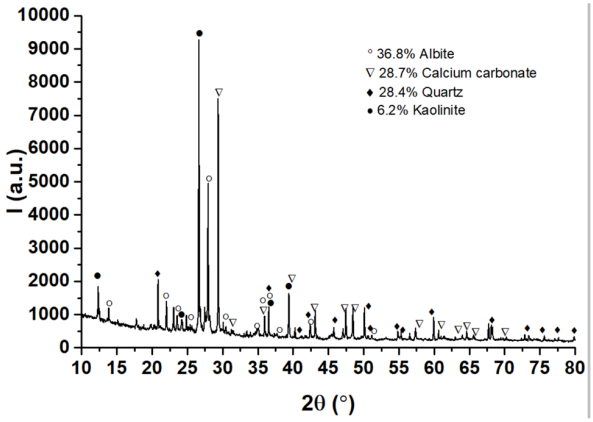

Figure 4. X-ray diffraction spectrum of the mortar. Albite ($NaAlSi_3O_8$—ICDD PDF4+#00-009-0466), quartz (SiO_2—ICDD PDF4+#01-070-3755), calcite ($CaCO_3$—ICDD PDF4+#04-023-8700), and kaolinite ($Al_2O_3 \cdot 2SiO_2 \cdot 2H_2O$_ICDD PDF4+#00-058-2028) mineral phases were identified.

Starting from the mass percentages provided by XRD, namely, albite ($NaAlSi_3O_8$) 36.8%; calcium carbonate ($CaCO_3$) 28.7%; quartz (SiO_2) 28.4%; and kaolinite ($Al_2Si_2O_5(OH)_4$) 6.2%, the value of 158.152 mg/'virtual mmole' of the homogenized mortar can be reached. This can be used to estimate the mass percentage per element: Na—5.37%, Al—8.48%, Si—26.78%, O—49.68%, Ca—7.27%, C—2.27%, H—0.15%.

The value of the mass percentage of carbon contained in the 'lumps and bumps' (henceforth called lumps), measured by elemental analysis, was 5.36%C. The nitrogen percentage of 0.1%N determined simultaneously with carbon enters the background threshold during thermal combustion in the EA (see Section 2.2.) and demonstrates that there is no contamination with organic material containing nitrogen inside lumps.

The value obtained for %C in lumps is 2–2.5 times higher than that for the homogenized mass of mortar, a value determined by XRD, namely 2.27%C (within the limits of experimental errors of the methods, and the material's inhomogeneity). But it is also 2–2.5 times lower than that for pure calcite (12%C).

A possible explanation is that lumps contain calcite/calcium carbonate together with other chemical elements, unidentifiable to the EA (such as Na, Al, Si, O, Ca, H), or, most likely, the material subjected to graphitization is a mixture of calcite from the time of hardening in construction, rehydrated calcite, secondary calcite, and/or geogenic calcite, together with some impurities from mortar, mentioned before.

The other analyses will bring new information to help define the chemical composition of the lumps as correctly as possible. This information is vital in the selection of the dating strategy and the interpretation of radiocarbon results.

3.2. Microstructural Analysis

The microstructure was characterized by SEM analysis. Figure 5 shows a highly inhomogeneous microstructure, with both large and small—and, probably, interconnected—pores and cracks, grains of various sizes, and entrapped air bubbles.

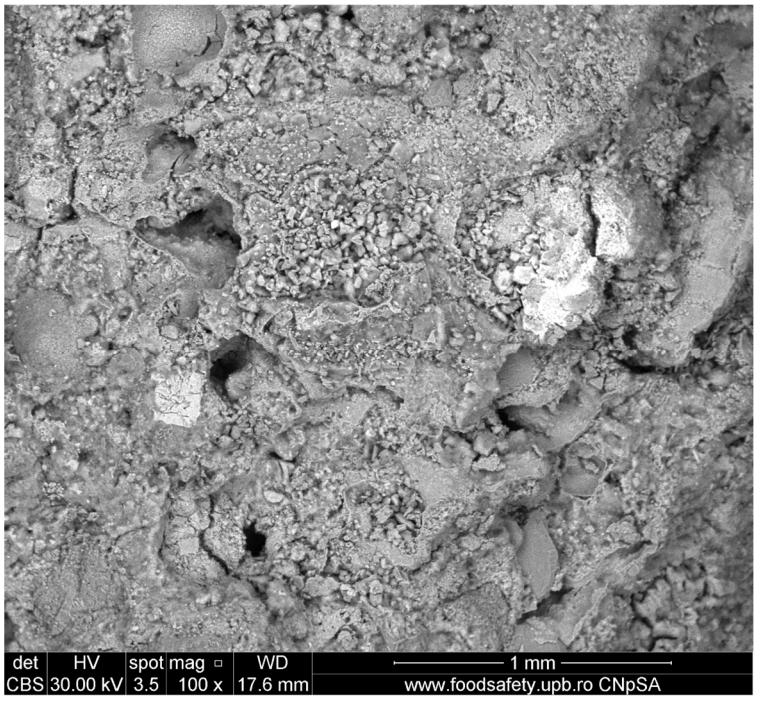

Figure 5. Inhomogeneous morphology of the sample surface captured by SEM (magnification 100×).

Figure 6 shows a large collection (a nest) of calcite grains with sizes less than 10 microns, which most probably resulted from the carbonation of a relatively big $Ca(OH)_2$/(CH) site.

Although small, calcite grains are, most of them, well developed with well-defined grain boundaries. The nest is surrounded by a dense and compact surface layer that could be a biofilm. These observations reinforce the conclusions from Section 2.1., excluding the presence of calcareous concretions in the mortar and even more so in the lumps (S5 calcareous concretions), as defined in the Section 1.

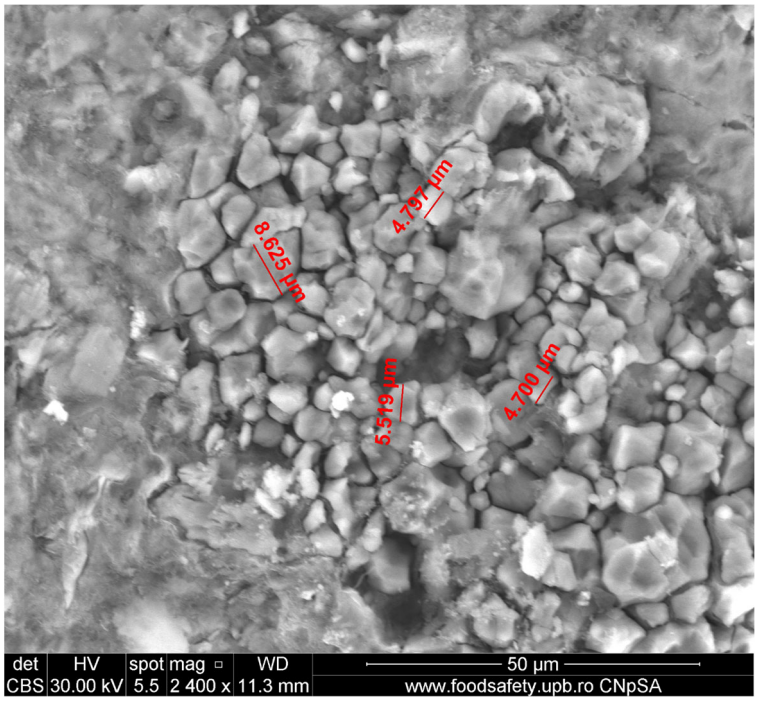

Figure 6. Nest of well-faceted $CaCO_3$ grains, typically less than 10 µm, captured by SEM (magnification 2400×).

A very small (less than 150 µm in size) silica grain was identified in the fracture, partially connected to the binder matrix, which contains mostly Ca and Si (as Al accounts for only 2.8%), distributed homogeneously—see Figure 7.

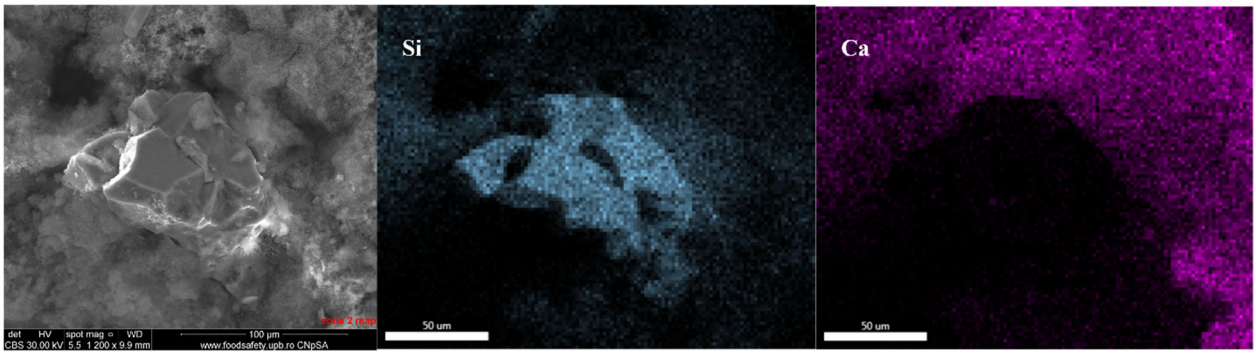

Figure 7. Silica grain, magnification 1200× (confirmed by EDAX maps).

Figure 8 presents an albite grain with partially filled channels on its surface; channels seem to be oriented, almost completely, in diagonal directions. EDAX maps confirm the existence of Na, Al, and Si oxides and spectral analysis confirms the existence of feldspar, identified in XRD (Figure 4).

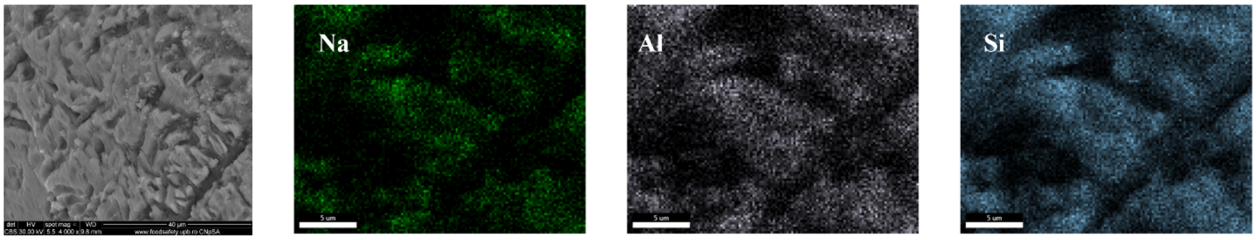

Figure 8. Eroded albite grain (magnification 4000×) confirmed by EDAX maps.

The existence of a calcium and phosphorus compound (Ca-P compound) is evidenced in Figure 9 along with variously sized pores, $CaCO_3$ lumps, quartz grains, and large areas of binder matrix. The Ca-P compound presents interconnected pores and is well embedded in the binder matrix. Its surface is covered with very small, probably calcium carbonate nodules and may represent a microfragment of bone, as suggested by literature data [32].

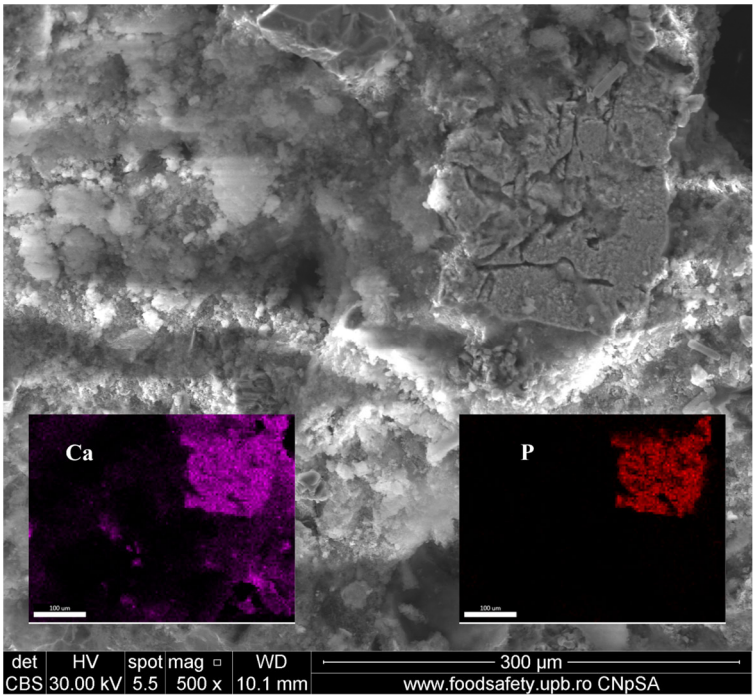

Figure 9. Ca–P compound showing interconnected channels (confirmed by EDAX maps as inset images)—magnification 500×.

The submicronic, spherical, and uniformly sized $CaCO_3$ grains identifiable in Figure 10 are most probably formed on a C-S(-H) bed (in atomic percentages: Ca—14.55, Si—2.09, Al—0.94). Their shape and size strongly contrast with the rest of the identified compacted, faceted-shaped, carbonate crystals, shown in Figure 6; a possible explanation for the different morphology is that their source may not be the carbonation of $Ca(OH)_2$. Judging by the small size, a credible hypothesis could be that they were formed by the carbonation of hydrated compounds, such as in S3 C-S-H carbonation, thus providing a proof of carbonation depth [12].

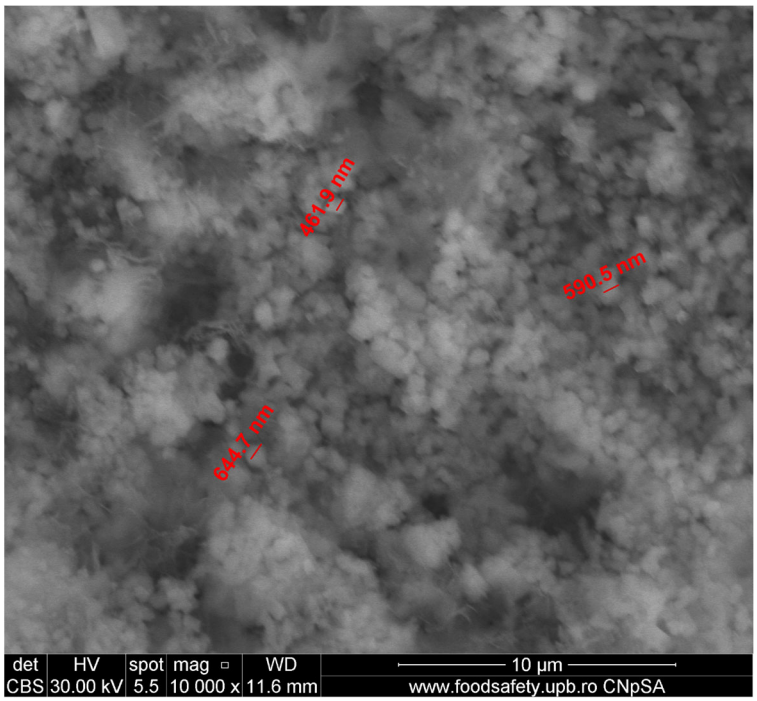

Figure 10. Layer of submicronic $CaCO_3$ grains, captured by SEM (magnification 10,000×).

The same submicronic $CaCO_3$ lumps can also be found on the surface of the gneiss aggregate—Figure 11.

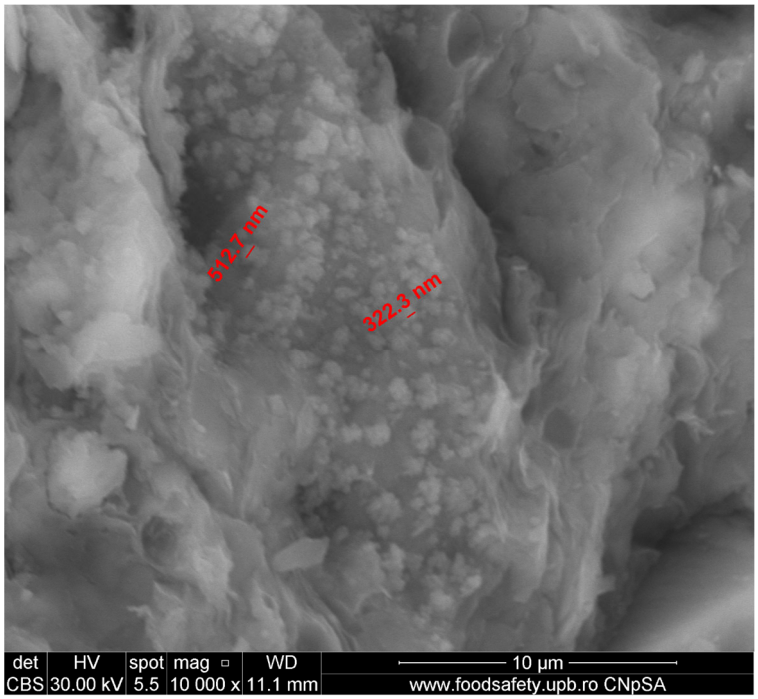

Figure 11. Submicronic $CaCO_3$ grains grown on the surface of the aggregate, captured by SEM (magnification 10,000×).

From SEM-EDAX analysis, it appeared that the microstructure of the mortar is inhomogeneous and crossed by a developed network of cracks, channels, and interconnected pores. It shows areas developed in the entire mass of the sample of calcite, as a result of the mortar hardening in the masonry, but also areas of lumps, clearly defined, which can be

isolated for further investigations. The latter were most likely formed by the carbonation over time of some 'nests' rich in slaked lime adherent to initial clusters of C-S-H/C-S-A-H hydrates. The two types of calcium carbonate/calcite, through the identified characteristics, come from the S2 pyrogenic calcite and S3 C-S-H carbonation calcite formation mechanisms, as presented in Section 1. No evidence of S1 geogenic calcite could be found, although its presence cannot be completely excluded in the absence of additional analyses such as cathodoluminescence and thin sections [33,34].

Submillimeter-sized quartz grains were spotted, which, along with the identified albite and the visible biotite $K(Mg,Fe)_3(AlSi_3O_{10})(F,OH)_2$, indicate an igneous origin of some of the fine aggregates. It is likely that locally available raw materials were used, because volcanic mountains are located at a few kilometers' distance. The small size of the SiO_2 grains could be due to (i) provenience, meaning that they may come from silt/other sediments (the hypothesis of fine grinding at that time could be rejected); (ii) larger grains having interacted with aluminosilicates via pozzolanic reactions, thus diminishing in size. Both hypotheses are equally probable.

3.3. ATR-FTIR Results

FTIR analysis, given in Figure 12, was performed in two areas: the first was a white area (red curve) and the second a grey area of the matrix (blue curve). Both curves have absorbance peaks at the same position; what differs is their band intensity ratio. For example, peaks at 1418, 873, and 711 cm^{-1}, respectively, can be attributed to calcite and have a higher amplitude for white areas (red curve), confirming that these areas contain more $CaCO_3$ than the grey areas. A broad, asymmetric feature in the range of 1200–900 cm^{-1} may indicate, with a high probability, the existence of albite feldspar, which was found in the XRD analysis (Figure 4); however, many minerals that come from granite/gneiss rocks containing Si-O (biotite, quartz) or kaolinite could be found in that area. The 520 and 441 cm^{-1} peaks identify the presence of quartz (or Si-O-Si in other minerals) in similar concentrations in the two samples. The broad band peaking at 3391 cm^{-1} is related to the existence of -OH groups; this may indicate the presence of adsorbed water and is directly related to the observed high porosity. This band will mask the peaks of the hydroxyl groups in biotite or kaolinite. No evidence of calcium hydroxide (CH) could be found, even in the ATR mode (CH could be identified by its sharp peak at 3640 cm^{-1}), as its signal can be hidden if the CH concentration is low enough.

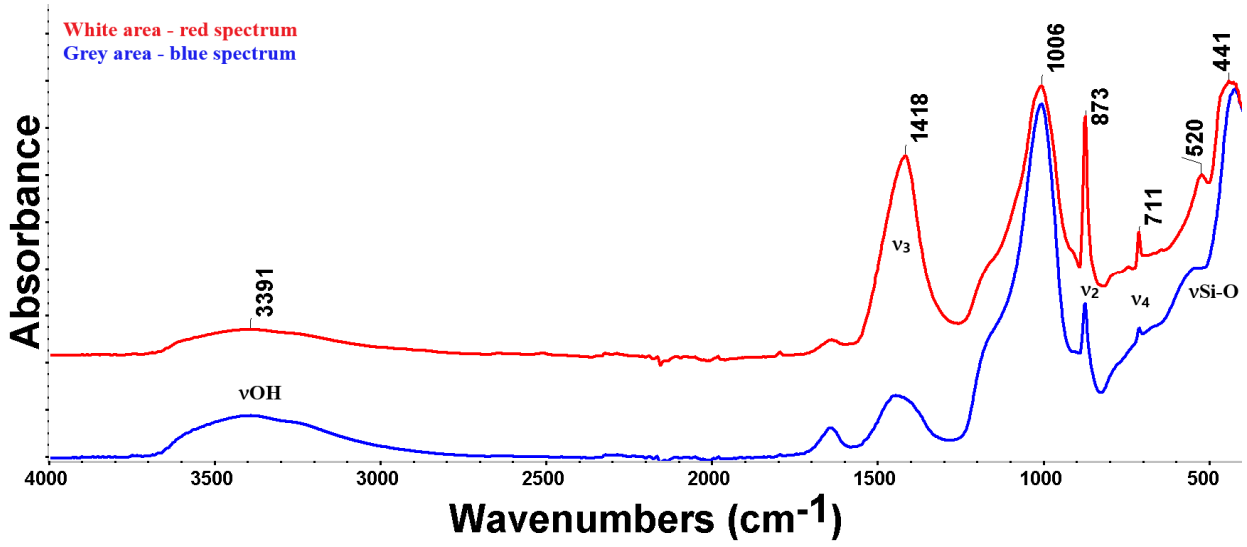

Figure 12. FTIR analyses on two areas of the specimen: white (red curve), grey (blue curve).

Previous literature data [19,35] were used to identify functional groups like CO_3^{2-} and Si-O and their characteristic FTIR peaks.

Differentiation between anthropogenic (pyrogenic) and geogenic $CaCO_3$ can be achieved using Fourier-transform infrared spectroscopy (FTIR) and the luminescence properties of calcium carbonate [36]. Both methods are based on different densities and distributions of atomic defects in the calcite crystal structure. In calcite, three major infrared absorption peaks are identified: ν_2 out-of-plane bending CO_3^{2-} (873 cm^{-1}), ν_3 asymmetric stretching CO_3^{2-} (1418 cm^{-1}), and ν_4 in-plane bending CO_3^{2-} (711 cm^{-1}). It was shown that the ratio between ν_2 and ν_4 bands' intensities reflects the order of the calcite crystal structure [37]. A high ratio is indicative of disorder in the crystal, i.e., the calcite is a pyrogenic, while at low values of the ratio (around 3), the calcite has a geogenic origin [37].

The analysis of Figure 12 according to the procedure given in [37] confirmed, based on the values of the ratio of the infrared absorption peaks, $\frac{\nu_2}{\nu_4} \cong 8$ for lumps and $\cong 5.7$ for grey areas (binder), that the origin of the calcite in the examined specimens is pyrogenic, highlighting the absence of S1 geogenic calcite. A higher value ratio for lumps suggests this material to be radiocarbon dated.

To confirm the existence of biotite, FTIR microscopy and maps were recorded. The red cross is placed, in Figure 13a, on the dark particle of about 0.5 mm size. FTIR maps corresponding to Si-O-Si groups and Al-O-Si groups, corroborated by the color, indicate that the particle is most likely made of biotite. Figure 13b shows an FTIR map plotted at 1005 cm^{-1}, corresponding to Si-O-Si groups, which could indicate biotite, having the highest absorbance in the area of the particle. Figure 13c gives the FTIR map recorded at 728 cm^{-1}, corresponding to Al-O-Si groups, which could indicate biotite, showing the highest absorbance in the area of the particle.

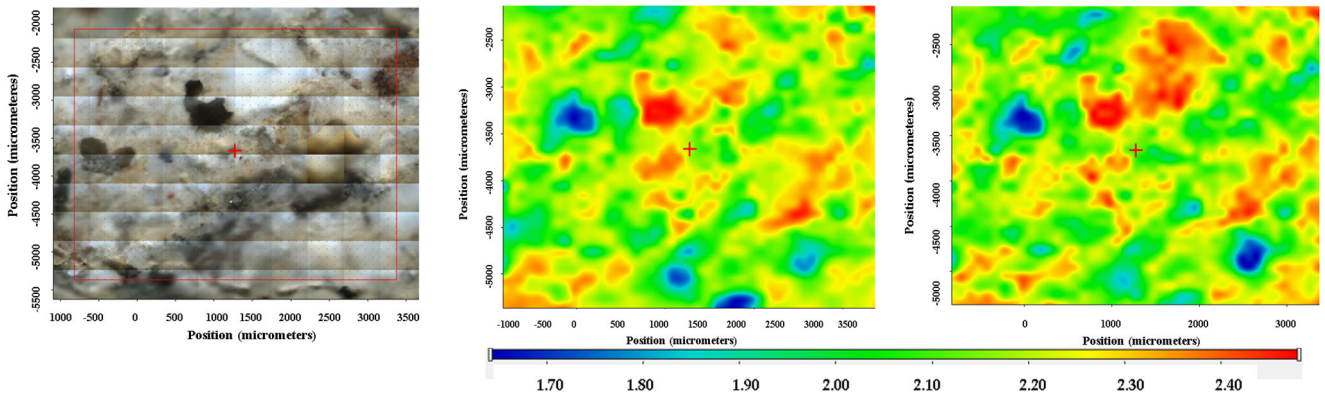

Figure 13. FTIR microscopy: (**a**) biotite particle; (**b**) biotite—1005 cm^{-1}; (**c**) biotite—728 cm^{-1}.

Note that the larger, white particle to its right side responds similarly, although weaker, indicating that is most probably made of albite.

FTIR-ATR analysis highlighted the structure of the compounds in the two areas. Calcite was identified both in the mortar binder and in the lumps. Its noticeably higher concentration in the lumps confirmed the previous results. What this investigation adds is the identification of biotite and the confirmation of the XRD results on kaolinite, quartz, and albite. They were identified in lumps, as impurities, along with calcite, partially explaining the lower %C percent determined in the EA.

If XRD and SEM-EDAX could disprove the hypothesis of lump-type formations originating from geogenic calcite (mechanism S1), FTIR-ATR draws attention to the fact that the $CaCO_3$ from C-S-H carbonation, controlled by a depth profile relationship, must

be considered (mechanism S3). The lack of calcium hydroxide demonstrates that the S4 $Ca(OH)_2$ recarbonation mechanism may be excluded.

3.4. Thermal Analysis Results

DSC-TGA analyses were performed on two samples, extracted from a white area (presumably with a higher concentration of calcite, denoted as N)—Figure 14—and from a grey area, denoted as G, Figure 15. Both samples performed similarly at heating; however, the amplitude of mass changes and recorded enthalpies are different.

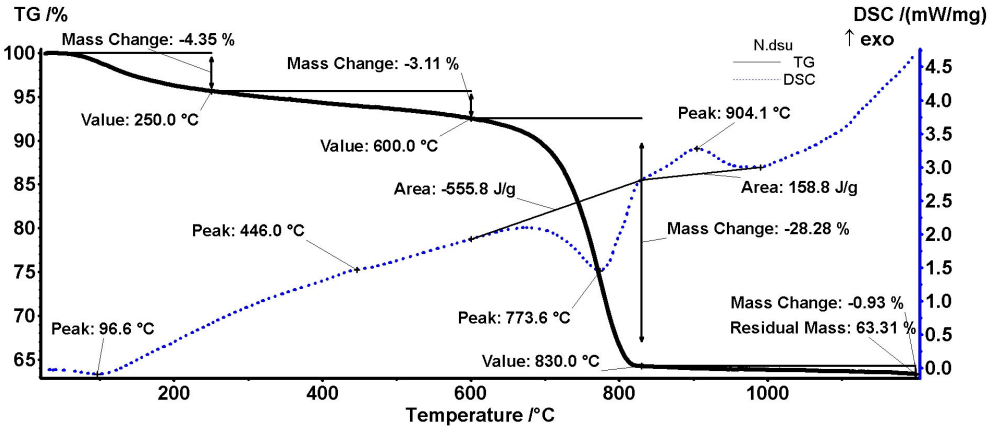

Figure 14. DSC-TGA results of the specimen extracted from a white area, presumably a lump.

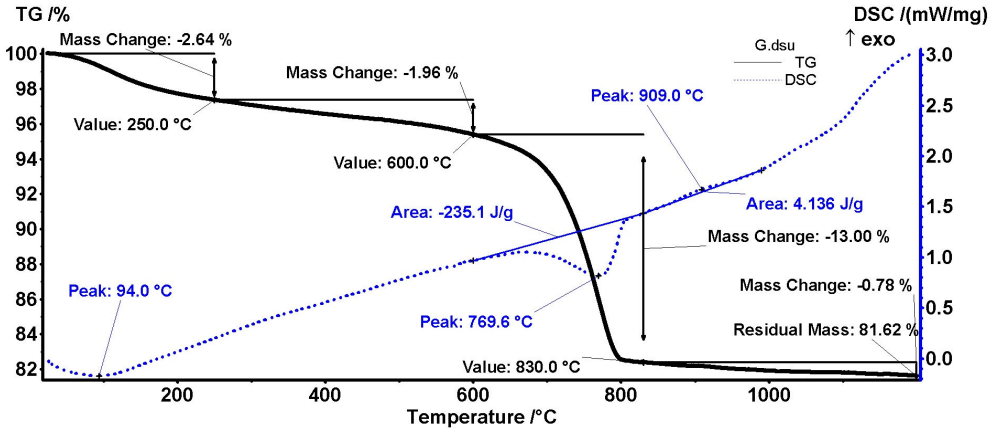

Figure 15. DSC-TGA results of a sample extracted from a grey area, presumably mortar binder.

As can be seen in Figure 14 for the white area (N sample, lumps), a first mass change occurs up to 250 °C (solid line for TGA) with a peak at 96.6 °C (dashed line for DSC). It corresponds to the elimination of adsorbed water, with the samples not being previously heated to 110 °C [37]. The second mass change occurs up to 600 °C. It corresponds to dehydroxylation of clay minerals or C-S-H/C-S-A-H, which is related in the DSC diagram to the peak at 446 °C [38]. No quartz transformation was identified at 573 °C, giving a sign of its absence in the lumps [39].

The most important loss in weight of 28.28% was recorded in the range of 600–830 °C, with a peak at 773.6 °C. This could be attributed to the decarbonation of the calcite from lumps [38]. Compared to the theoretical value of 43.97%, we found a percentage of around 64% calcium carbonate. A secondary peak was not identified at approx. 875 °C, generally associated with pure geogenic calcite or the polymorphic transformation of micaceous minerals, which is a sign of their absence [38,40]. An exothermic peak appears at around 904 °C and can be attributed to the final burning of organic wastes [41].

Concerning the grey area (Figure 15, G sample, mortar), the same losses at 94 °C, and up to 250 °C, can be found. Instead, the signal from approx. 446 °C disappeared. No quartz transformation was identified at 573 °C.

As for the decomposition of carbonates in the range of 600–830 °C, it is observed that this occurs at 769.9 °C. The dissociation temperature will depend primarily on their mineralogical structure, and also on the type and amount of impurities. Increasing the total content of aluminum, silicon, and iron oxides will lead to a decrease in the decomposition temperature, as a result of the formation of solid, unsaturated solutions in $CaCO_3$ [38]. Compared to the theoretical value of 43.97%, we found a percentage of around 30% calcium carbonate, with possible different origins. A secondary peak was not identified at approx. 875 °C. An exothermic peak appeared at around 909 °C [40].

As presented above, from the values recorded in Figures 14 and 15 (13% for G sample and 28% in N sample), the $CaCO_3$ concentration can be obtained: ~29% for G sample (grey area) and 64% for N sample, i.e., in white areas, confirming the XRD (Figure 4) and EA results.

A phase transformation can also be connected with lumps, at 446 °C, corresponding to the dehydroxylation of clay minerals or C-S-H/C-S-A-H. It does not show a phase transformation for quartz. The most important transformation is given in the range of 600–830 °C and is characteristic of calcium carbonate decomposition. Decomposition at a lower temperature in the mortar in comparison with lumps shows a greater 'flux' contribution of some mineral compounds. Geogenic calcite was not identified in this way either.

3.5. High-Resolution Gamma Spectrometric Analysis for Natural Radionuclides

The activity concentrations measured by gamma ray spectrometry in 80 g of mortar sample from Ulpia Traiana were ^{40}K: 581 ± 12 Bq·kg^{-1}; ^{232}Th (^{228}Ac): 28.5 ± 2.8 Bq·kg^{-1}; and ^{226}Ra: 32.7 ± 1.7 Bq·kg^{-1}, respectively. To verify the direct exposure to environmental factors, the existence of radioactive deposits of ^{137}Cs (T½ ≅ 30 years), in the last 75 years, was checked. The level was, after 4.2 days of measurements, below the detection limit, i.e., below 0.77 Bq·kg^{-1}.

According to the distribution map, for the ^{137}Cs inventory in this region (corresponding to May 1986, recalculated in 1993, 2016, and 2016–2018 from experimental data) [42], a value of 5 ÷ 10 kBq·sqm^{-1} or greater was expected to be found. The obtained value, within the limits of detection, may be a sign of indirect exposure or rather of a continuous wash-up by water, humidity, and wind. This analysis opens up a new direction for future exploration of the ruins of ancient fortresses, offering the opportunity to establish whether or not the investigated areas were exposed to external factors after 1945.

Concerning naturally occurring radionuclides (NORs), these values reveal low activity concentrations due to the low content in local limestone [43] or due to the specificity of other raw material sources in the area. This was the case for Bârzava (Romania), which afforded ^{40}K: 514 ± 21 Bq·kg^{-1}; ^{232}Th (^{228}Ac): 49 ± 4 Bq·kg^{-1}; and ^{226}Ra: 38 ± 8 Bq·kg^{-1} (less than 100 km away), and for Eastern Hungary: ^{40}K: 418 Bq·kg^{-1}; ^{232}Th (^{228}Ac): 32 Bq·kg^{-1}; and ^{226}Ra: 30 Bq·kg^{-1} [44,45]. The measured values for Ulpia Traiana were slightly lower than the average specific activity for Romania, which was ^{40}K: 635 Bq·kg^{-1}; ^{232}Th (^{228}Ac): 46 Bq·kg^{-1}; and ^{226}Ra: 54 Bq·kg^{-1} [46]. What was distinct for the above-mentioned locations was the ratio greater than 1 between ^{232}Th (^{228}Ac) and ^{226}Ra, revealing the materials used at Ulpia Traiana as being local materials. Volcanic tuffs or pozzolanic materials from the Roman Magmatic Province for enhancing the mortar's mechanical properties were not involved [47,48]. The findings from the other analyses, i.e., showing that local materials were used, were in this way substantiated.

3.6. Radiocarbon Dating

Considering all the interpretations of the previous analyses, a procedure for extracting small portions of lumps (a white material with the apparent consistency of calcite) under a microscope was followed. The total sample came from multiple sub-samples at several points in the material. After homogenization, we proceeded according to Section 2.2.

The calibration of the radiocarbon date (histogram) using the CHS method is presented in Figure 16.

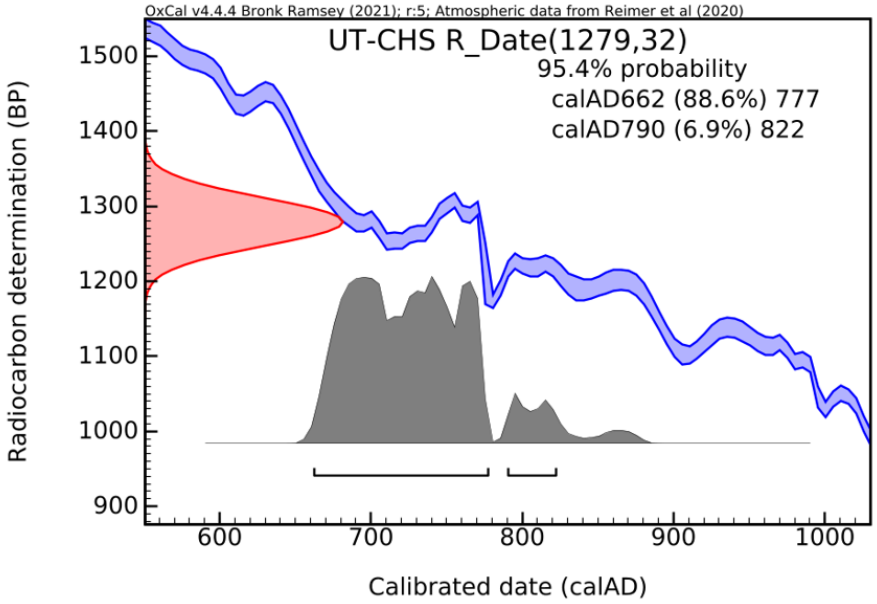

Figure 16. Histogram for lumps extracted from Ulpia Traiana mortar (UT), using CHS [29].

Based on the results obtained using the CHS, the age period falls within calAD 662–822, with a confidence level of 95.4%. In the CHS, only CO_2 from inorganic materials is released.

To verify the consistency of the radiocarbon date, a second round of dating was performed using the EA. In this case, without a prior pre-treatment of the samples, a radiocarbon date was obtained for all the forms in which carbon-14 is present (bio/organic and bio/inorganic). The second calibrated radiocarbon date is shown in Figure 17.

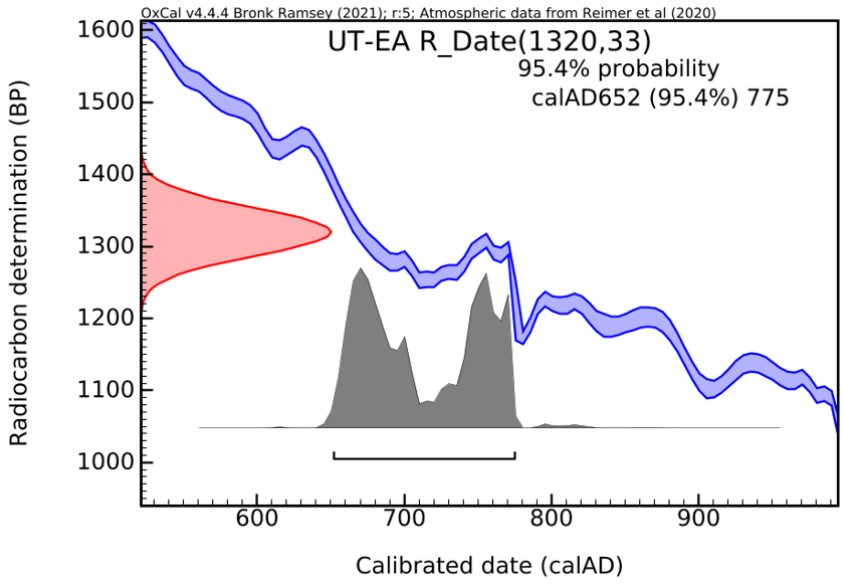

Figure 17. Histogram for dating lumps extracted from Ulpia Traiana mortar (UT), using EA [29].

This time, the age period falls within calAD 652–775, with a confidence level of 95.4%.

Both methods offered consistent results, reinforcing the reliability and accuracy of the dating outcome. Combining the CRA values by using the R_Combine function in OxCal [29] demonstrates the 'contemporaneity' of the samples. The most likely interval becomes narrower, namely between calAD 662 and 775 (Figure 18). The difference of approximately 100 years (within the limits of measurement errors) places it in the interval of 100–200 years, acceptable for the hardening of mortar in masonry.

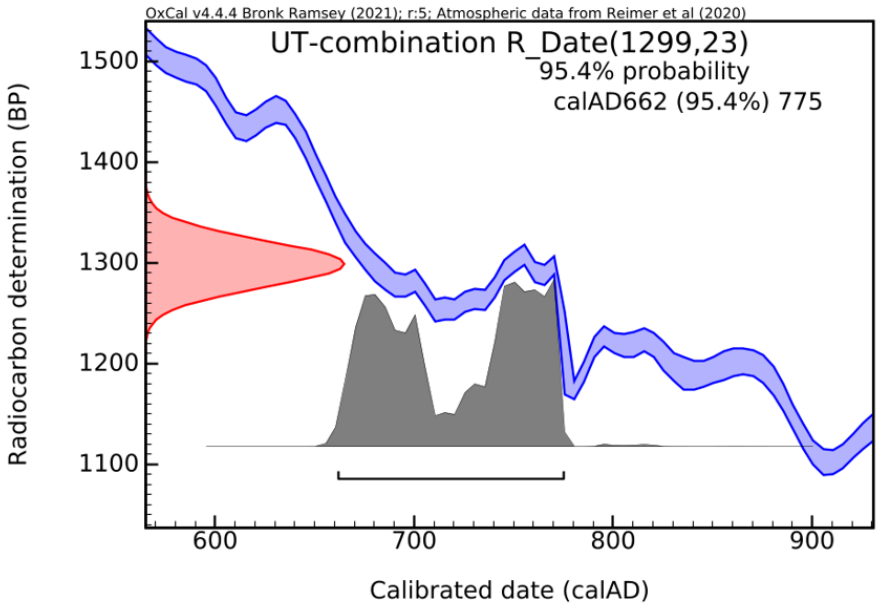

Figure 18. Histogram obtained by applying the R_combine function of OxCal Program [29].

The radiocarbon results confirm that it is not a modern intervention/late repair. The position of the sampling point excludes lateral contact producing C-14 exchanges during the lifetime of the monument [49], sustained by previous analyses. So, it may represent a real age, but not one supported by the archaeological or historical information accepted until now, even if 100–150 years are added (see above). It is most likely an apparent age depending on the distance from the surface, denoted by S2 pyrogenic calcite and S3 C-S-H carbonation mechanisms, as explained in Section 1. $CaCO_3$ from carbonated C-S-H/C-S-A-H, which could take up an unknown number of years, may be taken into consideration, if the degree of carbonation of the material is controlled by the carbonation depth (mechanism S3) [12]. As presented in the literature, the phenomenon of delayed mortar hardening is common to these water-resistant materials, leading to apparent ages more recent than its application in masonry [50]. Nowadays, similar materials in the cement class also exhibit this phenomenon. To modify the hardening period, retarders or accelerators, such as calcium lignosulfonate or sodium gluconate, are added [50,51].

Support for an apparently rejuvenated age or apparently obsolete one is given by the interpretations of the results obtained with the other investigation methods. The absence of geogenic calcite excludes the S1 mechanism stated in Section 1. A mortar hardened in 100–200 years (given the sampling position, from inside the plinth) and rejuvenated (through surface exposure after the statue reached the ruin phase) cannot be taken into consideration (mechanism S4 $Ca(OH)_2$ recarbonation).

4. Discussion

The integration of the results from Sections 3.1–3.6 involves two directions: firstly, the material characterization and the ageing processes undergone, and secondly, to what extent

the information confirms carbonation during hardening or if secondary/subsequent recrystallization has taken place over time, leading to rejuvenation. When S2 pyrogenic calcite and S3 C-S-H carbonation mechanisms overlap, as is the case, it cannot be a matter of rejuvenation but of a delay in the mortar hardening. Calcium carbonate in lumps was not formed exclusively by the S2 pyrogenic calcite mechanism, from the excess of slaked lime, but also by carbonation into the 'nested' hydrated forms of calcium silicates/aluminosilicates (mechanism S3). If C-S-H are present and then it is a hydraulic mortar, there are high chances that the carbonation process took a long time, making the radiocarbon date unreliable. Such assumptions on the presence/absence of possible geological calcium carbonate, unreacted lime lumps, as well a tendency of calcium carbonate to dissolve and reprecipitate with younger environmental carbon can be verified later using high-resolution instrumentation such as cathodoluminescence (CL) [33]. Also, optically stimulated luminescence (OSL) can be used to verify the correct choice of datable submicronic fractions [52].

Radiocarbon dating places the use of this mortar in the Medieval times (Middle Ages, 7–9th centuries, more precisely), which is several centuries after Aurelian's withdrawal from the Dacian provinces (271–272 AD).

If the radiocarbon date of the mortar taken from the plinth of the central statue in Forum Vetus had coincided with the time of its erection, i.e., 2nd century AD, the research would have been limited to characterizing the material (and obtaining a possible manufacturing formulation). In fact, the exact moment of construction is unknown but, the Trajan's forum was finished, according to an inscription, around 110 AD [53]. In the following period, a series of interventions were carried out in Forum Vetus, with the replacement of the cover limestone with marble, but there is no record of any work on Trajan's statue. After 153 AD, it was extended by Forum Novum [54]. The year 255 AD marks the retreat of the Huns with the abandonment and degradation of the colony. Thus, the construction of the plinth of the statue initially attributed to Trajan can be included in this period of approx. 150 years. The difference of centuries compared to the radiocarbon date, given that there were no modern interventions on this architectural element until now, raises new challenges, both technical and historical.

If the age is correctly represented by the radiocarbon date, there are two hypotheses: (i) a temporarily return of the Romans in the site, in which case the mortar is a Roman mortar, made with pozzolanic materials transported from the Italic Peninsula; (ii) resident craftsmen, either indigenous or migratory, possessed the knowledge and skills to develop lime mortars with locally available materials as in the case of basilica Torre de Palma [3]. Both hypotheses should be treated with caution, as there is not yet available evidence of any kind to support them.

If the age is 'apparent', beyond the threshold of 100–200 years generally accepted by the literature, the phenomenon of rejuvenation/delaying of the mortar hardening must be taken into account. Other hypotheses appear: (i) the sample was taken from the inner area of the plinth below the surface of the remaining part of the construction, leading to a slow exchange of the carbon-14 isotopic signature (thus modifying the radiocarbon date by the imminent contact with atmospheric CO_2; it is brought by meteoric waters or by organic and inorganic compounds in the air or water, of younger ages over time, as suggested by radiometric analyses) [55]; (ii) another hypothesis must take into account which hinges on the degree of carbonation with depth in the case of cementitious materials, commented on above.

Although a direct 'rejuvenation' of an older material with a younger C-14 (based on S1–S5 sources) is the most common hypothesis, a third one cannot be excluded: (iii) the mortar belongs to the time period of the return of the Romans, in the 10–13th centuries. The Medieval reuse of ancient ruins was a generalized phenomenon in the territory of

the former Empire. Not far from Sarmizegetusa, at Alba Iulia, it was established that the walls of the castle were fully reused for a Medieval fortress until the 13th century. Some towers were in operation even in the 14th century. Roman ruins can still be seen there, included in the structure of the palace of the Roman Catholic bishopric, together with numerous archaeological vestiges [56]. In fact, it is an 'ageing' that involves other directions of research: the slow exchange occurs this time between the same contaminating factors and geogenic sources of calcite (S1 geogenic calcite, S5 calcareous concretions) with an infinite radiocarbon age [57].

5. Conclusions

A set of analyses were applied on an ancient lime-based, porous concrete (denoted as mortar) extracted from the central part of Trajan's statue, Ulpia Traiana archaeological site, Romania.

This sample underwent complex characterization and we can offer the following conclusions, very useful in defining this ancient construction material:

Mainly albite, quartz, and calcium carbonate, along with kaolinite, were identified in XRD/SEM-EDAX performed on the binder matrix. Visible biotite grains of 1–2 mm in size were also observed, along with other aggregates (of various sizes and natures), all of them well-embedded in the binder matrix.

The 'specimen' surfaces and also fracture or fresh-cut surfaces contained white, up to millimeter-sized lumps made of more than 60% $CaCO_3$. This carbonate may appear due to carbonation of $Ca(OH)_2$ over time, generally within 100–200 years.

In addition, all surfaces, old or newly made by fracturing/cutting, were covered with a white, thin layer of carbonate, which appeared in SEM images as submicronic, spherical, and uniformly sized $CaCO_3$ grains. The origin of this carbonate may be the carbonation of the possible C-S-H hydrates formed within the binder matrix; this process, depending on depth, may have taken place in over 400 years. The pozzolanic reaction is suspected, as very small grains of silica (less than 150 μm in size) were detected.

FTIR analysis confirmed the presence of all previously identified minerals and suggested, based on the values for the ratio of the infrared absorption peaks, $\frac{\nu_2}{\nu_4} \cong 8$ for lumps and $\cong 5.7$ for binder, that the origin of the calcite in the examined specimens is pyrogenic (for reference, geogenic, natural calcite has a low ratio: $\frac{\nu_2}{\nu_4} \cong 3$). No calcium hydroxide was found, proving the lack of secondary calcite, much younger, in the formation.

Gamma spectrometry offers a new option for investigating a monument's dynamics, using ^{137}Cs as a radiotracer for over the last 75 years. Naturally occurring radionuclides such as ^{40}K, ^{232}Th (^{228}Ac), and ^{226}Ra strengthen the hypothesis of using local materials and not of bringing volcanic ash or pozzolanic materials from Italy.

Certain information was useful for the selection of datable material, namely, the so-called lumps.

The history of this statue is well-documented, with its construction being placed in the 2nd century AD, so the radiocarbon date was surprising.

Radiocarbon dating placed the material within the calAD 662–775 interval, with a confidence level of 95.4%, although questions arise as to whether this is a real age or an apparent one. What should have been a routine analysis, supported by other investigations, has become a case study that shows the limitations of radiocarbon dating.

The analyses demonstrated that there is no geogenic calcite, that the mortar has reached maturity, and that there are no phenomena of decarbonation with recarbonation to secondary calcite (within the limits of detection of the methods used). The fragment taken from the center of the exposed surface, the calcite to be dated, comes from the carbonation of excess slaked lime interconnected with the carbonation of C-S-H hydrates. The latter

process is time-dependent and governed by the distance from the outer surface, with the equilibrium being reached within hundreds of years. No organic remains were detected, which could lead to rejuvenation phenomena. In this case, the archaeological context and the evolution over time of the statue, which are well-known, could provide a starting point for better quantifying the phenomenon of delayed hardening of mortar over time.

Further laboratory investigations, such as analysis in thin sections, CL, or OSL, could provide additional arguments to validate the findings, especially serving to disprove the existence of secondary and geogenic calcite.

Author Contributions: Conceptualization, Z.D.G. and C.A.S.; Methodology, L.M., V.-A.S., D.-R.T., A.F., O.-C.O., R.C.F., I.R., M.L.M., I.M.S. and A.R.P.; Validation, Z.D.G. and C.A.S.; Formal Analysis, L.M., V.-A.S., D.-R.T., A.F., O.-C.O., R.C.F., I.R., M.L.M., I.M.S. and A.R.P.; Investigation, L.M., V.-A.S., D.-R.T., A.F., O.-C.O., R.C.F., I.R., M.L.M., I.M.S. and A.R.P.; Resources, C.A.S.; Data Curation, Z.D.G. and C.A.S.; Writing—Original Draft Preparation, Z.D.G. and C.A.S.; Writing—Review and Editing, C.A.S.; Visualization, C.A.S.; Supervision, Z.D.G.; Project Administration, Z.D.G. All authors have read and agreed to the published version of the manuscript.

Funding: The radiocarbon dating was carried out within the NUCLEU project, PN 23210201 and PN 23210102, financed by the Ministry of Research, Innovation, and Digitization, Romania. The experiments were carried out in a Tandetron™ 1MV accelerator from the Horia Hulubei National Institute for R&D in Physics and Nuclear Engineering (IFIN-HH) and were supported by the Romanian Government through the National Program for Infrastructure of National Interest (IOSIN funds).

Institutional Review Board Statement: Not applicable.

Data Availability Statement: Dataset available on request from the authors.

Acknowledgments: We would like to thank Felix Marcu, Director of the National Museum of Transylvania, for his reasoned opinions related to the historical and archaeological data from Ulpia Traiana.

Conflicts of Interest: The authors declare no potential conflicts of interest with respect to the research, authorship, and/or publication of this article.

Appendix A

X-ray diffraction (XRD) patterns were acquired using an Empyrean X-ray diffractometer (Malvern PANalytical, Cedar Park, TX, USA) with Ni-filtered CuKα radiation (λ = 1.5418 Å). Data collection was conducted over a 2θ range of 10° to 80°, employing a step size of 0.026° and a counting time of 255 seconds per step. Phase identification was performed using HighScore Plus software (version 3.0.e) in conjunction with the ICDD PDF-4+ 2023 database. Quantitative phase analysis was conducted using the Rietveld refinement method, incorporating a polynomial function for background modeling, a pseudo-Voigt function for peak shape characterization, and the Caglioti function to model peak broadening.

A QUANTA INSPECT F (FEI—PHILIPS, Eindhoven, The Netherlands) electron microscope equipped with a field emission gun with 1.2 nm resolution and an energy-dispersive X-ray (EDAX) detector with 133 eV MnK resolution was used to assess the surface morphology of the samples.

A Nicolet iS50 FTIR spectrometer equipped with an attenuated total reflection accessory (ATR) from Thermo Fisher Scientific, Waltham, MA, USA was used to record FTIR spectra in the range 400–4000 cm^{-1} with a resolution of 4 cm^{-1}. An FTIR microscope Nicolet iN10 MX was used to obtain the FTIR 2D maps in the range of 600 to 4000 cm^{-1}.

Netzsch (Selb, Germany) STA 449C Jupiter equipment was used to investigate the thermal behavior in the dynamic air atmosphere (50 mL/min) for each sample, in the temperature range of 20–1100 °C, with a heating speed of 10 °C/min.

To evaluate the activity concentrations of naturally occurring radionuclides ^{40}K, ^{238}U, ^{232}Th, and ^{226}Ra, a low-background coaxial p-type High-Purity Germanium (HPGe) detector was employed, featuring a relative efficiency of 35% and an energy resolution of 1.85 keV at 1332.5 keV, corresponding to ^{60}Co. High-resolution gamma spectrometric analysis for natural radionuclides was conducted using a cylindrical plastic container (7.5 cm in diameter and 2.7 cm in height) as the sample geometry.

Appendix B

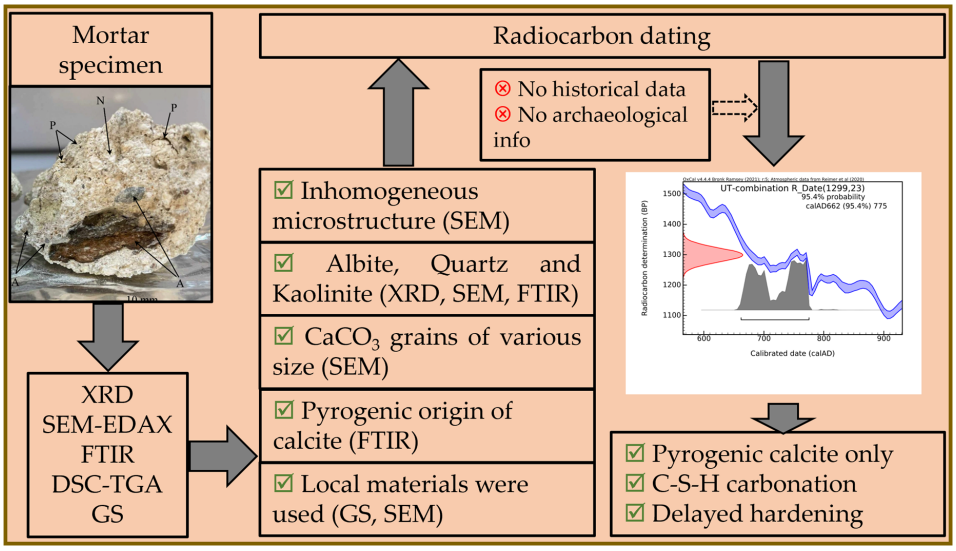

Figure A1. Schematic workflow of the study.

References

1. Artioli, G.; Secco, M.; Addis, A. The Vitruvian legacy: Mortars and binders before and after the Roman world. *EMU Notes Mineral.* **2019**, *20*, 151–202.
2. Lehner, M. *The Complete Pyramids*; Thames and Hudson: London, UK, 1997; ISBN 0-500-05084-8.
3. Tassios, T.P. Water supply of ancient Greek cities. *Water Sci. Technol. Water Supply* **2007**, *7*, 165–172. [CrossRef]
4. Vitruvius. *The Ten Books on Architecture*; with illustrations and original designs prepared under the direction of Warren, H.L. and Robinson, N., Jr.; Morgan, M.H., Translator; Harvard University Press: Cambridge, UK; Humphrey Milford Oxford University Press: London, UK, 1914; Available online: https://en.wikisource.org/wiki/Ten_Books_on_Architecture (accessed on 16 March 2021).
5. Zarzuela, R.; Luna, M.; Carrascosa, L.M.; Yeste, M.P.; Garcia-Lodeiro, I.; Blanco-Varela, M.T.; Cauqui, M.A.; Rodríguez-Izquierdo, J.M.; Mosquera, M.J. Producing C-S-H gel by reaction between silica oligomers and portlandite: A promising approach to repair cementitious materials. *Cem. Concr. Res.* **2020**, *130*, 106008. [CrossRef]
6. Hale, J.; Heinemeier, J.; Lancaster, L.; Lindroos, A.; Ringbom, Å. Dating Ancient Mortar. *Am. Sci.* **2003**, *91*, 130–137. [CrossRef]
7. Toffolo, M.B.; Regev, L.; Mintz, E.; Kaplan-Ashiri, I.; Berna, F.; Dubernet St Xin Yan Regev, J.; Boaretto, E. Structural characterization and thermal decomposition of lime binders allow accurate radiocarbon age determinations of aerial lime plaster. In *Radiocarbon, Proceedings of the Mortar Dating International Meeting, Pessac, France, 25–27 October 2018*; Cambridge University Press: Cambridge, UK, 2020; Volume 62, pp. 633–655. [CrossRef]
8. Campo, F.P.; Tua, C.; Biganzoli, L.; Pantini, S.; Grosso, M. Natural and enhanced carbonation of lime in its different applications: A review. *Environ. Technol. Rev.* **2021**, *10*, 224–237. [CrossRef]
9. Hajdas, I.; Maurer, M.; Röttig, M.B. Development of 14C dating of mortars at ETH Zurich. *Radiocarbon* **2020**, *62*, 591–600. [CrossRef]
10. Šavija, B.; Lukovic, M. Carbonation of cement paste: Understanding, challenges, and opportunities. *Constr. Build. Mater.* **2016**, *117*, 285–301. [CrossRef]

11. Arandigoyen, M.; Bicer-Simsir, B.; Alvarez, J.I.; Lange, D.A. Variation of microstructure with carbonation in lime and blended pastes. *Appl. Surf. Sci.* **2006**, *252*, 7562–7571. [CrossRef]
12. Bui, H.; Delattre, F.; Levacher, D. Experimental Methods to Evaluate the Carbonation Degree in Concrete—State of the Art Review. *Appl. Sci.* **2023**, *13*, 2533. [CrossRef]
13. Lindroos, A.; Ringbom, Å.; Heinemeier, J.; Hajdas, I.; Olsen, J. Delayed hardening and reactivation of binder calcite, common problems in radiocarbon dating of lime mortars. In *Radiocarbon, Proceedings of the Mortar Dating International Meeting, Pessac, France, 25–27 October 2018*; Cambridge University Press: Cambridge, UK, 2020; Volume 62, pp. 565–577. [CrossRef]
14. Daugbjerg, T.S.; Lindroos, A.; Heinemeier, J.; Ringbom, Å.; Barrett, G.; Michalska, D.; Hajdas, I.; Raja, R.; Olsen, J. A field guide to mortar sampling for radiocarbon dating. *Archaeometry* **2021**, *63*, 1121–1140. [CrossRef]
15. Toffolo, M.B. Radiocarbon dating of anthropogenic carbonates: What is the benchmark for sample selection? *Heritage* **2020**, *3*, 1416–1432. [CrossRef]
16. Toffolo, M.B.; Regev, L.; Dubernet, S.; Lefrais, Y.; Boaretto, E. FTIR-based crystallinity assessment of aragonite-calcite mixtures in archaeological lime binders altered by diagenesis. *Minerals* **2019**, *9*, 121. [CrossRef]
17. Martínez-García, C.; González-Fonteboa, B.; Carro-López, D.; Martínez-Abella, F. Pore Structure and Carbonation of Hydrated Lime Mortar with Mussel Shell Aggregate. In Proceedings of the International Conference on Bio-Based Building Materials, Belfast, UK, 26–28 June 2019.
18. Fort, R.; Varas-Muriel, M.J.; Ergenç, D.; Cassar, J.; Anastasi, M.; Vella, N.C. The technology of ancient lime mortars from the Żejtun Roman Villa (Malta). *Archaeol. Anthropol. Sci.* **2023**, *15*, 15. [CrossRef]
19. Maravelaki, P.N.; Theologitis, A.; Budak Unaler, M.; Kapridaki, C.; Kapetanaki, K.; Wright, J. Characterization of Ancient Mortars from Minoan City of Kommos in Crete. *Heritage* **2021**, *4*, 3908–3918. [CrossRef]
20. Nawrocka, D.; Michniewicz, J.; Pawlyta, J.; Pazdur, A. Application of radiocarbon method for dating of lime mortars. *Geochronometria. J. Methods Appl. Absol. Chronol.* **2005**, *24*, 109–115.
21. Mohanu, D. Causes and Specific Forms of Degradation. In *Corbii de Piatră. Interdisciplinary Study*; National University of Arts Printing: Bucharest, Romania, 2010; pp. 111–140.
22. Gomoiu, I.; Cojoc, R.; Enache, M.; Neagu, S.E.; Mohanu, D.; Mohanu, I. Microbial Ability to Colonize Mural Painting and Its Substrate. *Acta Phys. Pol. Ser. A* **2018**, *134*, 383–386. [CrossRef]
23. Zhu, J.; Qu, Z.; Liang, S.; Li, B.; Du, T.; Wang, H. Macroscopic and Microscopic Properties of Cement Paste with Carbon Dioxide Curing. *Materials* **2022**, *15*, 1578. [CrossRef]
24. Radulescu, I.; Calin, M.R. Reliability and performances of a high-purity gamma spectrometry system used for environmental measurements. *J. Radioanal. Nucl. Chem.* **2014**, *301*, 141–146. [CrossRef]
25. Pesce, G.L.A.; Ball, R.J.; Quarta, G.; Calcagnile, L. Identification, Extraction, and Preparation of Reliable Lime Samples for 14C Dating of Plasters and Mortars with the "Pure Lime Lumps" Technique. *Radiocarbon* **2012**, *54*, 933–942. [CrossRef]
26. Wacker, L.; Fulop, R.-H.; Hajdas, I.; Molnar, M.; Rethemeyer, J. A novel approach to process carbonate samples for radiocarbon measurements with helium carrier gas. *Nucl. Instrum. Methods Phys. Res. B* **2013**, *294*, 214–217. [CrossRef]
27. Stan-Sion, C.; Enachescu, M.; Petre, A.R.; Simion, C.A.; Calinescu, C.I.; Ghita, D.G. A new and compact system at the AMS laboratory in Bucharest. *Nucl. Instrum. Methods Phys. Res. Sect. B Beam Interact. Mater. At.* **2015**, *361*, 105–109. [CrossRef]
28. Wacker, L.; Christl, M.; Synal, H.A. BATS: A new tool for AMS data reduction. *Nucl. Instrum. Methods Phys. Res. B* **2010**, *268*, 976–979. [CrossRef]
29. Reimer, P.J.; Austin, W.E.N.; Bard, E.; Bayliss, A.; Blackwel, P.G.; Bronk Ramsey, C.; Butzin, M.; Cheng, H.; Edwards, R.L.; Friedrich, M.; et al. The IntCal20 Northern hemisphere radiocarbon age calibration curve (0–55 cal kBP). *Radiocarbon* **2020**, *62*, 725–757. [CrossRef]
30. Wacker, L.; Němec, M.; Bourquin, J. A revolutionary graphitization system: Fully automated, compact and simple. *Nucl. Instrum. Methods Phys. Res. B* **2010**, *268*, 931–934. [CrossRef]
31. Hajdas, I.; Lindroos, A.; Heinemeier, J.; Ringbom, Å.; Marzaioli, F.; Terrasi, F.; Passariello, I.; Capano, M.; Artioli, G.; Addis, A.; et al. Preparation and Dating of Mortar Samples—Mortar Dating Inter-Comparison Study (MODIS). *Radiocarbon* **2017**, *59*, 1845–1858. [CrossRef]
32. Nonni, S.; Marzaioli, F.; Secco, M.; Passariello, I.; Capano, M.; Lubritto, C.; Mignardi, S.; Tonghini, C.; Terrasi, F. 14C Mortar dating: The case of the medieval Shayzar Citadel, Syria. In *Radiocarbon, Proceedings of the 21st International Radiocarbon Conference, Paris, France, 9–13 July 2013*; Jull, A.J.T., Hatté, C., Eds.; Cambridge University Press: Cambridge, UK, 2016; Volume 55, pp. 514–525.
33. Toffolo, M.B.; Ricci, G.; Chapoulie, R.; Caneve, L.; Kaplan-Ashiri, I. Cathodoluminescence and laser-induced fluorescence of calcium carbonate: A review of screening methods for radiocarbon dating of ancient lime mortars. *Radiocarbon* **2020**, *62*, 545–564. [CrossRef]
34. Urbanová, P.; Boaretto, E.; Artioli, G. The state-of-the-art of dating techniques applied to ancient mortars and binders: A review. *Radiocarbon* **2020**, *62*, 503–525. [CrossRef]

35. Muller, C.M.; Pejcic, B.; Esteban, L.; Delle Piane, C.; Raven, M.; Mizaikoff, B. Infrared Attenuated Total Reflectance Spectroscopy: An Innovative Strategy for Analyzing Mineral Components in Energy Relevant Systems. *Sci. Rep.* **2014**, *4*, 6764. [CrossRef]
36. Calandra, S.; Conti, C.; Centauro, I.; Cantisani, E. Non-destructive distinction between geogenic and anthropogenic calcite by Raman spectroscopy combined with machine learning workflow. *Analyst* **2023**, *148*, 2861. [CrossRef]
37. Chu, V.; Regev, L.; Weiner, S.; Boaretto, E. Differentiating between anthropogenic calcite in plaster, ash and natural calcite using infrared spectroscopy: Implications in archaeology. *J. Archaeol. Sci.* **2008**, *35*, 905–911. [CrossRef]
38. Borsoi, G.; Santos Silva, A.; Menezes, P.; Candeias, A.; Mirão, J. Analytical characterization of ancient mortars from the archaeological Roman site of Pisões (Beja, Portugal). *Constr. Build. Mater.* **2019**, *204*, 597–608. [CrossRef]
39. Iordanidis, A.; Garcia-Guinea, J.; Strati, A.; Gkimourtzina, A.; Papoulidou, A. Thermal, mineralogical and spectroscopic study of plasters from three post-Byzantine churches from Kastoria (northern Greece). *J. Therm. Anal. Calorim.* **2011**, *103*, 577–586. [CrossRef]
40. Papadopoulou, D.N.; Lalia-Kantouri, M.; Kantiranis, N.; Stratis, J.A. Thermal and mineralogical contribution to the ancient ceramics and natural clays characterization. *J. Therm. Anal. Calorim.* **2006**, *84*, 39–45. [CrossRef]
41. Font, R. Decomposition of Organic Wastes: Thermal Analysis and Evolution of Volatiles. *Handb. Therm. Anal. Calorim.* **2018**, *6*, 339–397.
42. Blebea-Apostu, A.-M.; Margineanu, R.M.; Duliu, O.G.; Persa, D.; Gomoiu, M.C. ^{137}Cs distribution on the territory of Romania 30 years after Chernobyl accident. *Environ. Monit. Assess.* **2023**, *195*, 848. [CrossRef]
43. Calin, M.R.; Radulescu, I.; Chiper, D.; Barna, C.; Cimpeanu, C. Chemical characterization and radiation exposure from the natural radioactivity in Romanian building materials. *Radiochim. Acta* **2017**, *106*, 413–425. [CrossRef]
44. Florea, N.; Duliu, O.G. Rehabilitation of the Barzava Uranium Mine Tailings. *J. Hazard. Toxic. Radioact. Waste* **2013**, *17*, 230–236. [CrossRef]
45. Papp, Z. Natural radioactivity in the soils of some eastern counties of Hungary. *Radiat. Prot. Dosim.* **2010**, *141*, 56–63. [CrossRef]
46. Blebea-Apostu, A.-M.; Margineanu, R.M.; Persa, D.; Dumitras, D.-G.; Gomoiu, M.C.; Duliu, O.G. The distribution of natural radionuclides ^{40}K, ^{228}Ac and ^{226}Ra on Romanian Territory: A radiometric study. *Environ. Monit. Assess.* **2024**, *196*, 186. [CrossRef]
47. Botticelli, M.; Calzolari, L.; DeVito, C.; Mignardi, S.; Medeghini, L. Aqua Traiana, a Roman Infrastructure Embedded in the Present: The Mineralogical Perspective. *Minerals* **2021**, *11*, 703. [CrossRef]
48. Medeghini, L.; Calzolari, L.; Capriotti, S.; Bernabale, M.; De Vito, C.; Giustini, M.; Pettiti, I.; Dell'Agli, G.; Spiridigliozzi, L.; Antonacci, A.; et al. How the materials knowledge of Roman mortars could be helpful for the production of future materials: The case of the Aqua Traiana aqueduct (Rome, Italy). *Cem. Concr. Res.* **2024**, *179*, 107478. [CrossRef]
49. Pons-Branchu, E.; Caffy, I.; Delque-Kolic, E.; Dumoulin, J.-P.; Dumont, E.; Madikita, S.; Bultez, G.; Malnar, D.; Monvoisin, G.; Querleux, J.; et al. Radiocarbon dating of urban secondary carbonate deposits: Site effect and implication for chronology: Case study of Paris and Versailles Palace fountains. In *Radiocarbon, Proceedings of the 3rd Radiocarbon in the Environment Conference, Gliwice, Poland, 5–9 July 2021*; Cambridge University Press: Cambridge, UK, 2022; Volume 64, pp. 1323–1332. [CrossRef]
50. Bae, Y.H.; Ahn, Y.-R.; Jun, Y.; Yim, H.J. Evaluating the effect of retarder on cement hydration and setting delay under hot weather curing condition using non-destructive methods. *Mater. Struct.* **2024**, *57*, 224. [CrossRef]
51. Yamada, K.; Ichikawa, T.; Arai, H.; Yasukochi, T.; Endo, K. Study on the mechanisms of retardation of cement hydration by zinc and acceleration of hardening by sodium aluminate from crystallographic phase analysis. *J. Mater. Cycles Waste Manag.* **2024**, *26*, 3596–3608. [CrossRef]
52. Panzeri, L.; Maspero, F.; Anna Galli, A.; Emanuela Sibilia, E.; Martini, M. Luminescence and radiocarbon dating of mortars at Milano-Bicocca Laboratories. *Radiocarbon* **2020**, *62*, 657–666. [CrossRef]
53. Petolescu, C.C. *Inscripţii Latine Din Dacia (ILD)*; Editura Academiei Române: Bucharest, Romania, 2005.
54. Țentea, O.; Olteanu, B.C. Decorating Overlapping Buildings: A Domus and Palmyrene Temple at Colonia Dacica Sarmizegetusa. *Theor. Rom. Archaeol. J.* **2020**, *3*, 6. [CrossRef]
55. Lichtenberger, A.; Lindroos, A.; Raja, R.; Heinemeier, J. Radiocarbon analysis of mortar from Roman and Byzantine water management installations in the Northwest Quarter of Jerash, Jordan. *J. Archaeol. Sci. Rep.* **2015**, *2*, 114–127. [CrossRef]
56. Marcu-Istrate, D. *Catedrala Romano-Catolică "Sfântul Mihail" și Palatul Episcopal Din Alba Iulia: Cercetări Arheologice (2000–2002)*; Alba Iulia: Altip, Romania, 2009; pp. 45–53.
57. Asscher, Y.; van Zuiden, A.; Elimelech Ch Gendelman, P.; Uzi 'Ad Sharvit, J.; Secco, M.; Ricci, G.; Artioli, G. Prescreening Hydraulic Lime-Binders for Disordered Calcite in Caesarea Maritima: Characterizing the Chemical Environment Using FTIR. In *Radiocarbon, Proceedings of the the Mortar Dating International Meeting, Pessac, France, 25–27 October 2018*; Cambridge University Press: Cambridge, UK, 2020; Volume 62, pp. 527–543. [CrossRef]